Desalination and Water Treatment
www.deswater.com

doi: 10.1080/19443994.2015.1070761

57 (2016) 15603–15611
July

Taylor & Francis
Taylor & Francis Group

Statistical optimization of Reactive Red 141 removal by heterogeneous photo–Fenton reaction using $ZnFe_2O_4$ oxide prepared by microwave irradiation

Chayene G. Anchieta[a], Guilherme L. Dotto[a], Marcio A. Mazutti[a], Raquel C. Kuhn[a], Gabriela C. Collazzo[a], Osvaldo Chiavone-Filho[b], Edson L. Foletto[a,*]

[a]*Department of Chemical Engineering, Federal University of Santa Maria, Santa Maria 97105-900, Brazil, emails: chaya_36@hotmail.com (C.G. Anchieta), guilherme_dotto@yahoo.com.br (G.L. Dotto), marciomazutti@gmail.com (M.A. Mazutti), raquelckuhn@yahoo.com.br (R.C. Kuhn), gabrielacollazzo@gmail.com (G.C. Collazzo), Fax: +55 55 32208030; email: efoletto@gmail.com (E.L. Foletto)*

[b]*Department of Chemical Engineering, Federal University of Rio Grande do Norte, Natal 59072-970, Brazil, email: osvaldochiavonefilho@gmail.com*

Received 16 February 2015; Accepted 5 July 2015

ABSTRACT

A statistical optimization of Reactive Red 141 (RR141) removal by heterogeneous photo–Fenton reaction using $ZnFe_2O_4$ particles was performed. $ZnFe_2O_4$ oxide was synthesized by microwave-assisted solvothermal route and characterized by X–ray diffraction, Fourier transform infrared spectroscopy, and N_2 adsorption–desorption isotherms. This material was used as a catalyst for the removal of RR141 dye from aqueous solution. Statistical optimization for the RR141 removal was performed using a 2^{4-1} fractional experimental design, followed by the response surface methodology. Effects of pH, reaction time, dye concentration, and H_2O_2 concentration were evaluated. $ZnFe_2O_4$ particles presented a mesoporous structure with surface area of 65 $m^2\ g^{-1}$. It was found that the more adequate conditions for the RR141 dye removal were pH 2.0, reaction time of 60 min, dye concentration of 60 mg L^{-1}, and H_2O_2 concentration of 10 mM. In these conditions, 90% of color removal was achieved. The results demonstrate that the $ZnFe_2O_4$ oxide is an efficient catalyst for the removal of RR141dye from aqueous solution through the heterogeneous photo–Fenton reaction.

Keywords: Central composite design; Photo–Fenton; Dye; Statistical optimization; $ZnFe_2O_4$

1. Introduction

Dye-containing effluents from the textile industries can cause various environmental impacts, since they contain suspended solids, higher values of oxygen chemical demand, dyes, and other soluble substances [1]. Particularly, dye molecules are difficult to be removed from the effluents, because they are characterized by high chemical stability and low degradability. It is recognized that the advanced oxidation processes (AOPs) are an emerging technology to remove dyes from aqueous effluents [2]. Among the AOPs, heterogeneous Fenton reaction is one of the most promising technologies to remove organic

*Corresponding author.

compounds [3–6]. In this technique, iron-based materials can be separated and recovered from the aqueous solutions by a magnetic field for further reutilization due to their magnetic properties [7]. Several iron-based materials, such as $FeVO_4$, $CuFe_2O_4$, Fe_3O_4, α–Fe_2O_3, and α–FeOOH have been applied as catalysts in Fenton reaction in order to remove the pollutant compounds [8–11]. Recently, $ZnFe_2O_4$ oxide has received attention due to its high catalytic potential to degrade organic pollutants [12–14].

Different process conditions should be studied to obtain satisfactory results in the effluent treatment using Fenton reaction [11,15]. Among them, parameters such as pH, H_2O_2 concentration, dye concentration, and H_2O_2: Fe molar ratio are fundamental factors [15–17]. Therefore, in order to decrease the operational costs, these variables should be optimized. Classical methods to evaluate the factors that affect the photo–Fenton reaction require many experiments and do not consider interaction effects. In this context, response surface methodology (RSM) is an alternative method to minimize the experiments' number and evaluate the interaction effects. In addition, statistical models to represent the desired response as a function of studied variables can be generated [18–23].

In this work, $ZnFe_2O_4$ oxide was used as a catalyst in the heterogeneous photo–Fenton reaction to remove RR141 dye from aqueous solution. $ZnFe_2O_4$ catalyst was synthesized by microwave-assisted solvothermal method and characterized by different techniques. Effects of pH (1.16–4.00), reaction time (10.0–76.8 min), dye concentration (40.0–76.8 mg L^{-1}), and H_2O_2 concentration (20.0–60.0 mM) were evaluated in order to optimize the RR141 dye removal by heterogeneous photo–Fenton reaction. Statistical optimization was performed using a 2^{4-1} fractional design, followed by the RSM.

2. Experimental

2.1. Materials and reagents

The analytical grade reagents used in this work were acquired from Synth and Sigma-Aldrich: sulfuric acid (H_2SO_4), sodium hydroxide (NaOH), hydrogen peroxide (H_2O_2), zinc nitrate ($Zn(NO_3)_2{\cdot}6H_2O$), iron nitrate ($Fe(NO_3)_3{\cdot}9H_2O$), ethylene glycol ($C_2H_4(OH)_2$), and sodium acetate (CH_3COONa). Reactive Red 141 dye (Procion Red H-E7B; CAS number 61,931–52–0; $C_{52}H_{34}O_{26}S_8Cl_2N_{14}$; soluble in water) was provided by a textile company from southern Brazil. This dye was herein selected, because it is largely employed in textile industries and is a common pollutant in textile effluents [24,25].

2.2. Synthesis and characterization of $ZnFe_2O_4$ oxide

$ZnFe_2O_4$ particles were synthesized by the microwave-assisted solvothermal route, which was recently developed in our laboratory [26]. $Zn(NO_3)_2{\cdot}6H_2O$ and $Fe(NO_3)_3{\cdot}9H_2O$ were used as precursor salts and ethylene glycol was used as a solvent. The stoichiometric ratio using Zn:Fe was 1:2. In brief, 4.0 mmol of $Zn(NO_3)_2{\cdot}6H_2O$ and 8.0 mmol of $Fe(NO_3)_3{\cdot}9H_2O$ were dissolved in 120 mL of ethylene glycol under constant agitation, along with the addition of 60.0 mmol of sodium acetate (CH_3COONa). After that, the solution was transferred to a Teflon reactor and submitted to microwave irradiation (MARS 6 Microwave, ESP 1500 plus, USA) under the following conditions: temperature of 230°C, power of 600 W, and time of 30 min. Finally, the precipitate was removed, washed several times with deionized water and oven dried at 110°C for 24 h. $ZnFe_2O_4$ catalyst was characterized by X–ray diffraction (XRD), Fourier transform infrared spectroscopy (FTIR), and N_2 adsorption–desorption isotherms (BET). The diffractogram of $ZnFe_2O_4$ oxide was obtained by means of a Powder diffractometer (Rigaku, Miniflex 300, Japan), equipped with Ni–filtered Cu-Kα radiation ($\lambda = 1.54051$ Å), with $2\theta = 25°$–$65°$. The diffractometer was operated with a step size of 0.03° and a count time of 0.9 s per step, receiving slits at 30 kV and 10 mA. The average crystallite size (D, Å) was determined by the Scherrer equation (Eq. (1)) [27], where K is the Scherrer constant (0.90), $h_{1/2}$ is the width at half height of the more intense peak and θ is the position of this peak (in this work, $2\theta = 35.36°$).

$$D = \frac{K\lambda}{h_{1/2}\cos\theta} \quad (1)$$

FTIR spectrum was recorded by a Shimadzu IR-Prestige-21 spectrometer. Potassium Bromide (KBr) pellet was prepared with 10 mg of $ZnFe_2O_4$ and 300 mg of KBr [28]. FTIR spectrum was measured in the range 4,000–400 cm^{-1}. Surface area (BET) and pore size distribution of $ZnFe_2O_4$ catalyst were obtained from the N_2 adsorption–desorption isotherms at 77 K with P/P_0 ranging from 0.00 to 0.99 (Micromeritics, ASAP 2020, USA) [29].

2.3. Photo–Fenton assays

Photo–Fenton assays were performed in a 100 mL batch glass reactor (internal diameter of 5 cm and height of 6 cm) equipped with a spiral commercial fluorescent lamp (Empalux, 85 W, 65 lumens W^{-1}).

The distance between the liquid surface and the lamp was 15 cm. The dye solutions (50 mL) with different initial concentrations (according to the statistical optimization; see Table 1) had the pH adjusted (according to the experimental design; Table 1) and, 0.025 g of $ZnFe_2O_4$ was added. It is known that the acidic condition is required for a promising performance of the Fenton reaction [14,26]. The solutions were stirred in the dark at 100 rpm and 25°C, until reaching the adsorption equilibrium. Then, H_2O_2 was added to solution (according to the experimental design; Table 1) and light irradiation was further employed. All experimental conditions employed in this work were based on previous works [14,26]. Samples were collected at different time intervals, filtered, and measured at a maximum wavelength of 543 nm (Shimadzu–UV 1,800 spectrophotometer, Japan). The removal efficiency (E, %) was determined as a function of color removal, according to Eq. (2), where A_0 is the initial absorbance and A is the absorbance at reaction time t.

$$E(\%) = \frac{(A_0 - A)}{A_0} \times 100 \quad (2)$$

2.4. Experimental design

RR141 removal by heterogeneous photo–Fenton reaction was investigated using a 2^{4-1} fractional experimental design, followed by the RSM. Effects of pH, reaction time, dye concentration, and H_2O_2 concentration on the decolorization of RR141 dye were evaluated.

Firstly, a 2^{4-1} fractional design was used in order to verify the individual effects of pH (2.00 and 4.00), reaction time (10.0 and 60.0 min), dye concentration (40.0 and 60.0 mg L^{-1}), and H_2O_2 concentration (20.0 and 60.0 mM). These levels and factors were determined by preliminary experimental tests according to the literature [1,10,11,17,30–32]. The real and coded values of the investigated variables are shown in Table 1. Posteriorly, the dye removal efficiency (E) was optimized using a central composite rotatable design (2^3 with three central and six axial points) [18,21,33,34]. The effects of reaction time (from 43.2 to 76.8 min), pH (from 1.16 to 2.84), and dye concentration (from 43.2 to 76.8 mg L^{-1}) were evaluated. The real and coded values of the variables using a central composite rotatable design are presented in Table 2. The response (E) was represented as a function of independent variables according to a quadratic polynomial equation (Eq. (3)) [18], where a is the constant coefficient, b_i is the linear coefficient, b_{ij} is the interaction coefficient, b_{ii} is the quadratic coefficient, and x_i, x_j are the coded values of the variables.

$$E = a + \sum_{i=1}^{n} b_i x_i + \sum_{i=1}^{n} b_{ii} x_i^2 + \sum_{i=1}^{n-1} \sum_{j=i+1}^{n} b_{ij} x_i x_j \quad (3)$$

The statistical significance of the nonlinear regression was determined by Student's test, the second order model equation was evaluated by Fischer's test and the proportion of variance was explained by the model obtained [18]. Experimental runs were performed in random order and the results were analyzed using Statistic version 9.1 (Statsoft, USA) software.

3. Results and discussion

3.1. Characterization of $ZnFe_2O_4$ oxide

Fig. 1 shows the X–ray diffractogram (a) and FTIR spectrum (b) of $ZnFe_2O_4$ oxide prepared by microwave-assisted solvothermal method.

The X–ray diffractogram (Fig. 1(a)) shows that $ZnFe_2O_4$ oxide presented a cubic and single phase structure, according to the Joint Committee on Powder Diffraction Standards (JCPDS), card no. 89–1,012. The diffraction peaks at 2θ of 30.05°, 35.36°, 42.78°, 52.96°,

Table 1
Coded and real (in parentheses) variables and results for the 2^{4-1} fractional experimental design

Run	$[H_2O_2]$/(mM)	[Dye]/(mg L^{-1})	pH	t/(min)	E_{exp}/(%)[a]	E_{rep}/(%)[a]
1	1 (60.0)	1 (60.0)	1 (4.00)	1 (60.0)	1.93	2.03
2	1 (60.0)	1 (60.0)	–1 (2.00)	–1 (10.0)	50.39	50.98
3	1 (60.0)	–1 (40.0)	1 (4.00)	–1 (10.0)	0.55	0.62
4	1 (60.0)	–1 (40.0)	–1 (2.00)	1 (60.0)	75.00	74.06
5	–1 (20.0)	1 (60.0)	1 (4.00)	–1 (10.0)	2.20	1.90
6	–1 (20.0)	1 (60.0)	–1 (2.00)	1 (60.0)	90.62	89.04
7	–1 (20.0)	–1 (40.0)	1 (4.00)	1 (60.0)	1.45	1.50
8	–1 (20.0)	–1 (40.0)	–1 (2.00)	–1 (10.0)	47.50	52.05

[a]E_{exp} = removal efficiency of the experiment and E_{rep} = removal efficiency to its replicate.

Table 2
Coded and real (in parentheses) variables and results for the central composite rotatable design

Run	pH	[Dye]/(mg L^{-1})	t/(min)	E_{exp}/(%)[a]
1	1 (2.50)	1 (70.0)	1 (70.0)	47.26
2	1 (2.50)	1 (70.0)	–1 (50.0)	37.50
3	1 (2.50)	–1 (50.0)	1 (70.0)	70.01
4	1 (2.50)	–1 (50.0)	–1 (50.0)	51.32
5	–1 (1.50)	1 (70.0)	1 (70.0)	79.31
6	–1 (1.50)	1 (70.0)	–1 (50.0)	75.57
7	–1 (1.50)	–1 (50.0)	1 (70.0)	71.83
8	–1 (1.50)	–1 (50.0)	–1 (50.0)	32.50
9	–1.68 (1.16)	0 (60.0)	0 (60.0)	56.98
10	1.68 (2.84)	0 (60.0)	0 (60.0)	50.98
11	0 (2.00)	–1.68 (43.2)	0 (60.0)	49.68
12	0 (2.00)	1.68 (76.8)	0 (60.0)	24.53
13	0 (2.00)	0 (60.0)	–1.68 (43.2)	54.11
14	0 (2.00)	0 (60.0)	1.68 (76.8)	79.22
15	0 (2.00)	0 (60.0)	0 (60.0)	89.00
16	0 (2.00)	0 (60.0)	0 (60.0)	90.00
17	0 (2.00)	0 (60.0)	0 (60.0)	89.50

[a]E_{exp} = removal efficiency of the experiment.

56.78° and 62.20° can be attributed to the diffraction planes of (2 2 0), (3 1 1), (4 0 0), (4 2 2), (5 1 1), and (4 4 0), respectively. No impurity was detected. The average crystallite size (D) determined by the Scherrer equation (Eq. (1)) was 177 Å. The FTIR spectrum of $ZnFe_2O_4$ (Fig. 1(b)) shows bands at 3,440, 1,640, 570, and 440 cm^{-1}. The bands at 3,440 and 1,640 cm^{-1} can be assigned to vibrations of water molecules on the $ZnFe_2O_4$ surface. The bands visualized at 570 cm^{-1} (Zn–O) and 440 cm^{-1} (Fe–O) indicate the $ZnFe_2O_4$ phase formation [35,36].

Nitrogen adsorption–desorption isotherms of $ZnFe_2O_4$ sample and its pore size distribution curve are shown in Fig. 2.

Fig. 2(a) shows the N_2 adsorption–desorption isotherms, which can be categorized as type III, indicating a predominantly mesoporous structure (20 Å < pore size < 500 Å) [37]. The pore size distribution curve (Fig. 2(b)) displays a wide distribution, with predominance in the mesoporous region (20 Å < pore size < 500 Å). This mesoporous characteristic can be attributed to the pore voids among the agglomerate particles. The surface area, average pore size, and total pore volume of the $ZnFe_2O_4$ sample were 65 $m^2\ g^{-1}$, 170 Å, and 0.301 $cm^3\ g^{-1}$, respectively.

3.2. Fractional experimental design

RR141 dye was removed from aqueous solutions by the photo–Fenton reaction using $ZnFe_2O_4$ as catalyst. Table 1 shows the results obtained using a 2^{4-1} fractional experimental design in order to evaluate pH, reaction time, dye concentration, and H_2O_2 concentration on the RR141 dye removal efficiency (E).

Based on the results presented in Table 1, a Pareto chart (Fig. 3) was utilized in order to verify the effects of the independent variables on the RR141 dye removal efficiency. Fig. 3 shows that all independent variables were significant ($p < 0.05$) in relation to the removal efficiency. The pH, dye concentration, and H_2O_2 concentration have negative effects on the response, meaning that the lower the pH, dye concentration, and H_2O_2 concentration the better the removal efficiency. On the other hand, obviously the time had a positive effect on the response.

Pareto chart shows that the pH value had the largest influence on the dye removal efficiency, presenting a negative effect, which means that the decolorization efficiency decreases as the solution pH increases. The Fenton technology applies the combination of H_2O_2 and Fe^{2+} in an acidic aqueous medium (pH ≤ 3), producing hydroxyl reactive radicals ($HO^{\bullet}$), which are effective in the oxidation of pollutant molecules [38,39]. RR141 dye removal efficiency was also improved by the contact time increase and dye concentration decrease (Table 1). The H_2O_2 concentration decrease causes an increase in the removal efficiency, because at higher H_2O_2 concentrations, the $HO^{\bullet}$ radical can be eliminated due to the generation of hydroxyperoxide radicals ($HO_2^{\bullet}$), which is less reactive [39,40]. Therefore the results of a 2^{4-1} fractional design were used to define the levels and

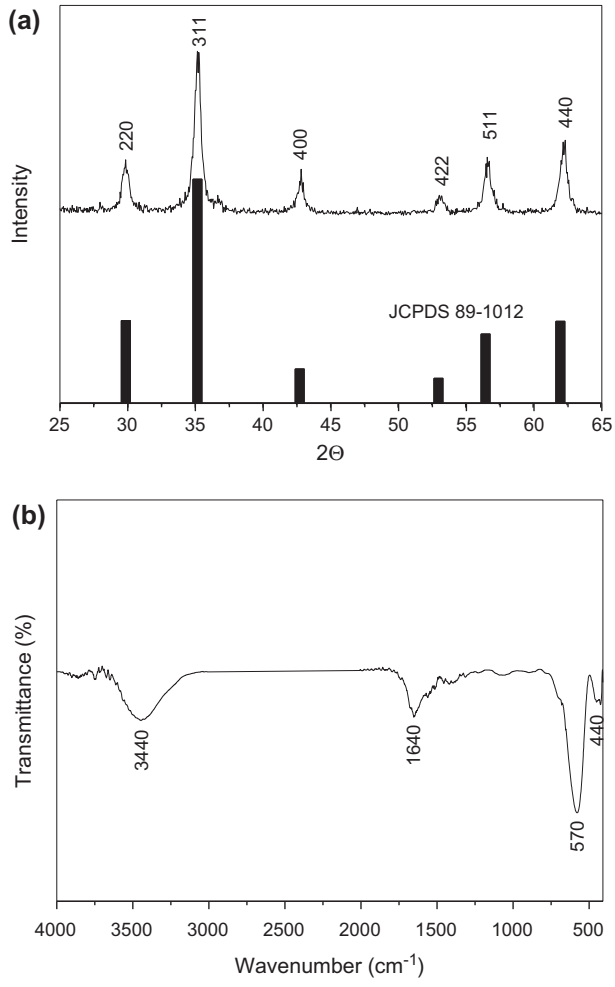

Fig. 1. X–ray diffractogram (a) and FTIR spectrum (b) of $ZnFe_2O_4$ oxide.

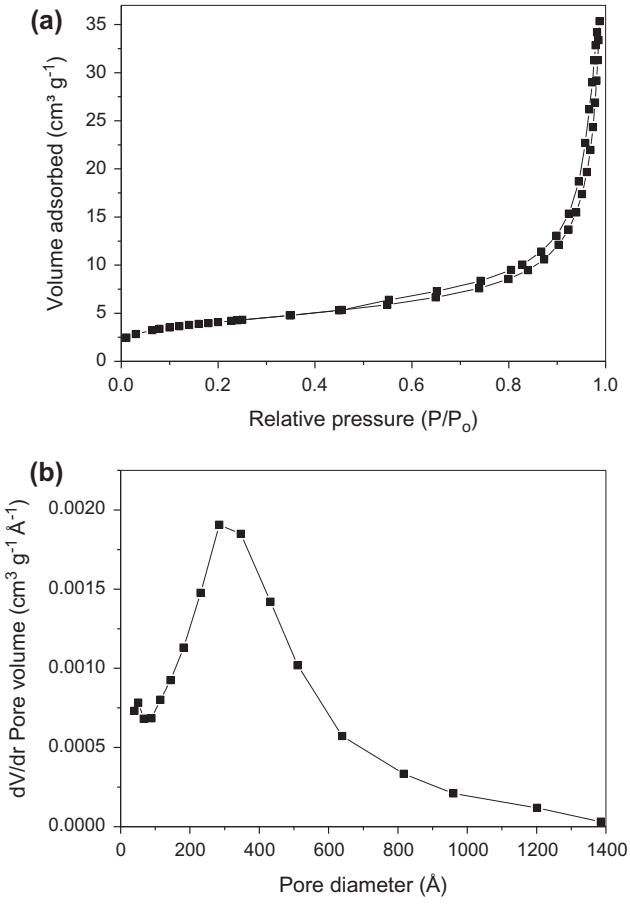

Fig. 2. N_2 adsorption–desorption isotherms (a) and pore size distribution (b) of $ZnFe_2O_4$ oxide.

factors of central composite rotatable design (Table 2), which was used to optimize the RR141 dye removal. Since pH, reaction time, and dye concentration were the most influential factors, they were the variables studied.

3.3. Optimization of RR141 dye removal

In order to obtain the optimal reaction conditions, the removal efficiency (E) was optimized using a central composite rotatable design (2^3 with three central and six axial points). Table 2 shows the levels, variables, and results of this experimental design.

Pareto chart (Fig. 4) was used to verify the significance of pH, reaction time, and dye concentration on the RR141 dye removal efficiency.

Fig. 4 demonstrates that the quadratic effects of dye concentration and pH have a significant effect at

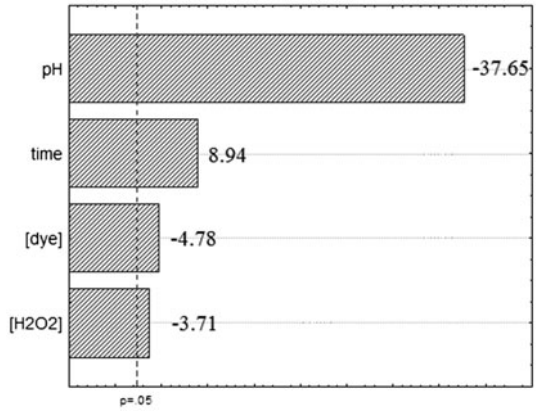

Fig. 3. Pareto chart for the removal efficiency as a function of the independent variables using fractional experimental design.

95% of confidence ($p < 0.05$) on the RR141 dye removal efficiency. In addition, the interaction effect of pH vs. dye concentration and the linear effect of

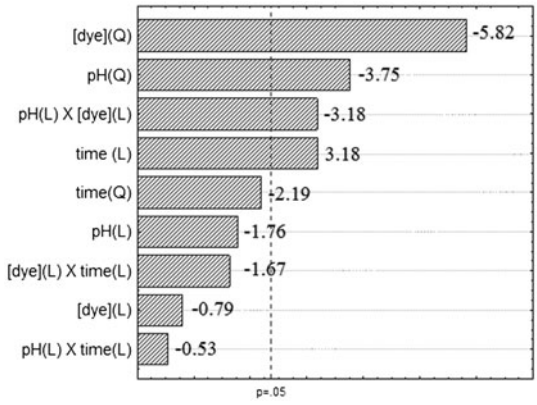

Fig. 4. Pareto chart for the removal efficiency as a function of the independent variables.

reaction time also were significant ($p < 0.05$). Based on the results from Table 2, a statistical polynomial quadratic model was proposed to represent the removal efficiency (E) as a function of significant variables. These coded (Eq. (4)) and uncoded models (Eq. (5)) are presented below:

$$E_{coded} = 89.7 - 10.82\,pH^2 - 16.79\,Dye^2 + 8.33\,Time - 10.89\,pH \times Dye \quad (4)$$

$$E_{uncoded} = -1441.4 + 316.5\,pH - 43.29\,pH^2 + 27.65\,Dye - 0.17\,Dye^2 + 12.5\,Time - 2.18\,pH \times Dye \quad (5)$$

For a more adequate representation of the experimental data, the statistical coded model (Eq. (4)) was used. The significance and prediction of this model were evaluated by the analysis of variance (ANOVA) and Fischer F test. The determination coefficient was 0.91, showing that the model was significant, and the calculated F value ($F_{calc} = 23.4$) was 7.8 times higher than the standard F value ($F_{std} = 3.0$), showing that the model was predictive. The model reliability was evaluated by the predicted vs. observed values. Fig. 5 shows that the experimental data followed the tendency of the coded model.

Eq. (4) was used to generate a response surface shown in Fig. 6, which represents the RR141 dye removal efficiency as a function of the independent variables (pH and dye concentration). It can be visualized in Fig. 6 that the percentage removal of RR141 dye shows a parabolic behavior in relation to the pH and dye concentration, being that the maximum values were attained at the central point. Thus, the optimal conditions for RR141 dye removal from aqueous solutions were at pH of 2.00, dye concentration of 60.0 mg L^{-1}, and reaction time of 60 min. Under these conditions, the removal efficiency was about 90%. Recently, RR141 dye has been degraded by photo–Fenton process using iron-based catalysts [14,41]. $ZnFe_2O_4$ particles were prepared by solvothermal conventional method using two diols as solvents (1,4 butanediol and ethylene glycol) [14] and FeZSM-5 zeolite particles [41] have demonstrated high efficiency (>85% after 60 min of

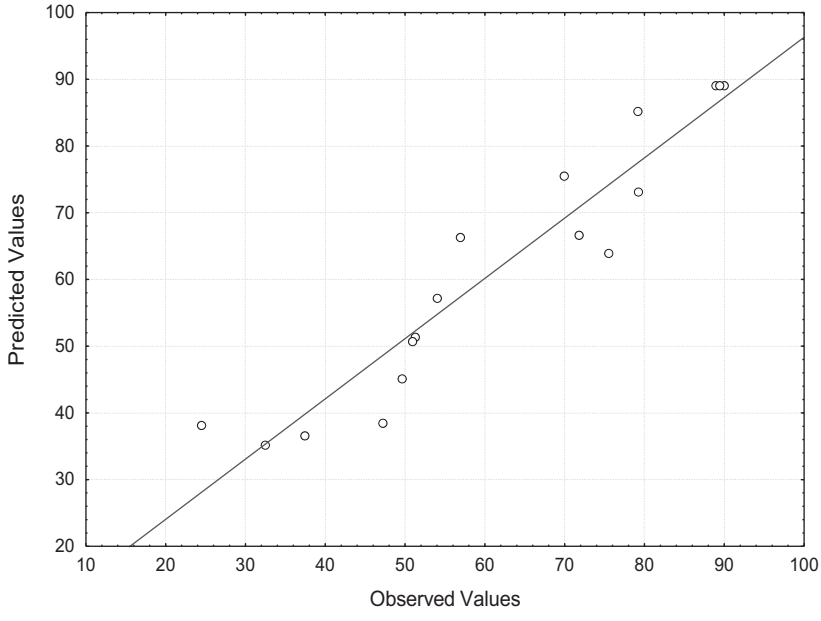

Fig. 5. Predicted vs. observed values for the removal efficiency.

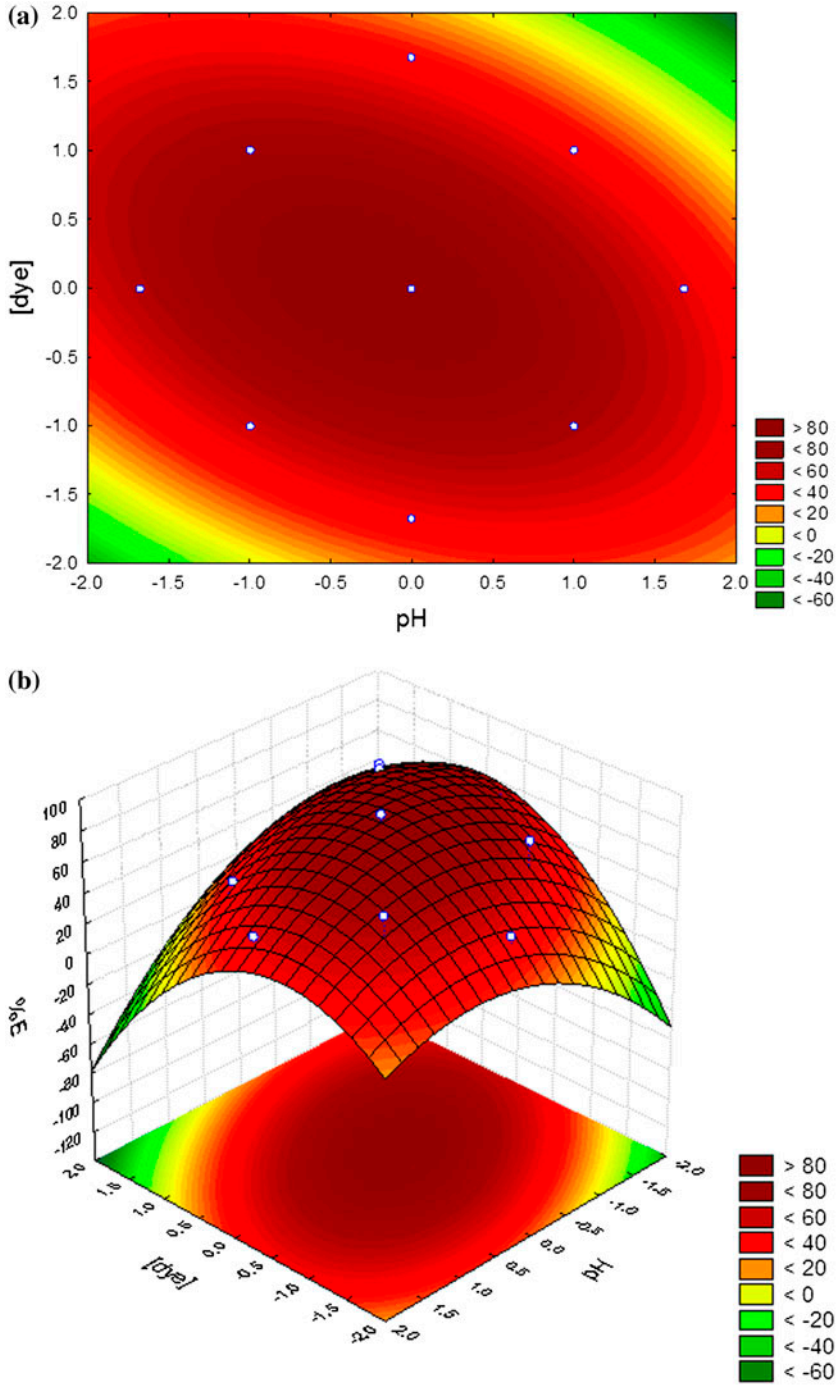

Fig. 6. Contour surface (a) and response surface (b) for the removal efficiency as a function of the independent variables.

reaction time) in the RR141 dye removal from aqueous solution. Therefore the results obtained in this work were highly satisfactory and can be attributed to the mesoporous structure of $ZnFe_2O_4$ particles.

4. Conclusions

This work demonstrates that the $ZnFe_2O_4$ catalyst can be successfully synthesized by the microwave-assisted solvothermal route under the following

conditions: temperature of 230˚C, power of 600 W, and time of 30 min. $ZnFe_2O_4$ spinel presented a mesoporous structure with satisfactory catalytic activity for the Reactive Red 141 dye degradation. According to statistical optimization, it was possible to provide a significant and predictive model to represent the removal efficiency of RR141 dye as a function of the independent variables. In the better assay, around 90% of RR141 dye was removed at pH of 2.00, dye concentration of 60.0 mg L^{-1}, and reaction time of 60 min. These results demonstrate that the photo–Fenton reaction using $ZnFe_2O_4$ oxide as catalyst is an adequate technology to remove the RR141 dye from aqueous solutions.

Acknowledgments

The authors would like to thank CAPES (Coordination for the Improvement of Higher Education Personnel) and CNPq (National Council for Scientific and Technological Development) for the financial support.

References

[1] R. Ansari, Z. Mosayebzadeh, Application of polyaniline as an efficient and novel adsorbent for azo dyes removal from textile wastewaters, Chem. Pap. 65 (2011) 1–8.
[2] P. Oancea, V. Meltzer, Kinetics of tartrazine photodegradation by UV/H_2O_2 in aqueous solution, Chem. Pap. 68 (2014) 105–111.
[3] L. Djeffal, S. Abderrahmane, M. Benzina, S. Siffert, Efficiency of natural clay as heterogeneous Fenton and photo-Fenton catalyst for phenol and tyrosol degradation, Desalin. Water Treat. 52 (2014) 2225–2230.
[4] Q. Wang, S. Tian, J. Cun, P. Ning, Degradation of methylene blue using a heterogeneous Fenton process catalyzed by ferrocene, Desalin. Water Treat. 51 (2013) 5821–5830.
[5] Y. Aşçı, Decolorization of Direct Orange 26 by heterogeneous Fenton oxidation, Desalin. Water Treat. 51 (2013) 7612–7620.
[6] S. Yue, F. Qiyan, L. Xiangdong, Application of response surface methodology to optimize degradation of polyacrylamide in aqueous solution using heterogeneous Fenton process, Desalin. Water Treat. 53 (2015) 1923–1932.
[7] C. Yao, Q. Zeng, G.F. Goya, T. Torres, J. Liu, H. Wu, M. Ge, Y. Zeng, Y. Wang, J.Z. Jiang, $ZnFe_2O_4$ nanocrystals: Synthesis and magnetic properties, J. Phys. Chem. C 111 (2007) 12274–12278.
[8] K. Hanna, T. Kone, G. Medjahdi, Synthesis of the mixed oxides of iron and quartz and their catalytic activities for the Fenton-like oxidation, Catal. Commun. 9 (2008) 955–959.
[9] S. Rahim Pouran, A.A. Abdul Raman, W.M.A. Wan Daud, Review on the application of modified iron oxides as heterogeneous catalysts in Fenton reactions, J. Cleaner Prod. 64 (2014) 24–35.
[10] Y. Wang, H. Zhao, M. Li, J. Fan, G. Zhao, Magnetic ordered mesoporous copper ferrite as a heterogeneous Fenton catalyst for the degradation of imidacloprid, Appl. Catal., B: Environ. 147 (2014) 534–545.
[11] X. Zhang, Y. Ding, H. Tang, X. Han, L. Zhu, N. Wang, Degradation of bisphenol A by hydrogen peroxide activated with $CuFeO_2$ microparticles as a heterogeneous Fenton-like catalyst: Efficiency, stability and mechanism, Chem. Eng. J. 236 (2014) 251–262.
[12] X. Li, Y. Hou, Q. Zhao, L. Wang, A general, one-step and template-free synthesis of sphere-like zinc ferrite nanostructures with enhanced photocatalytic activity for dye degradation, J. Colloid Interface Sci. 358 (2011) 102–108.
[13] J. Wu, W. Pu, C. Yang, M. Zhang, J. Zhang, Removal of benzotriazole by heterogeneous photoelectro-Fenton like process using $ZnFe_2O_4$ nanoparticles as catalyst, J. Environ. Sci. 25 (2013) 801–807.
[14] C.G. Anchieta, A. Cancelier, M.A. Mazutti, S.L. Jahn, R.C. Kuhn, A. Gündel, O. Chiavone-Filho, E.L. Foletto, Effects of solvent diols on the synthesis of $ZnFe_2O_4$ particles and their use as heterogeneous photo-Fenton catalysts, Materials 7 (2014) 6281–6290.
[15] A.M.F.M. Guedes, L.M.P. Madeira, R.A.R. Boaventura, C.A.V. Costa, Fenton oxidation of cork cooking wastewater—Overall kinetic analysis, Water Res. 37 (2003) 3061–3069.
[16] N.N. Mahamuni, Y.G. Adewuyi, Advanced oxidation processes (AOPs) involving ultrasound for waste water treatment: A review with emphasis on cost estimation, Ultrason. Sonochem. 17 (2010) 990–1003.
[17] T. Mackuľak, M. Smolinska, P. Olejnikova, J. Prousek, A. Takačova, Reduction of ostazine dyes' photodynamic effect by Fenton reaction, Chem. Pap. 66 (2012) 156–160.
[18] R.H. Myers, D.C. Montgomery, Response Surface Methodology: Process and Product Optimization using Designed Experiments, second ed., John Wiley & Sons, New York, NY, 2002.
[19] I. Arslan-Alaton, A.B. Yalabik, T. Olmez-Hanci, Development of experimental design models to predict Photo-Fenton oxidation of a commercially important naphthalene sulfonate and its organic carbon content, Chem. Eng. J. 165 (2010) 597–606.
[20] V. Homem, A. Alves, L. Santos, Amoxicillin degradation at ppb levels by Fenton's oxidation using design of experiments, Sci. Total Environ. 408 (2010) 6272–6280.
[21] G.L. Dotto, V.M. Esquerdo, M.L.G. Vieira, L.A.A. Pinto, Optimization and kinetic analysis of food dyes biosorption by *Spirulina platensis*, Colloids Surf., B: Biointerfaces 91 (2012) 234–241.
[22] W. Li, B. Li, W. Ding, J. Wu, C. Zhang, D. Fu, Response surface methodology as a tool to optimize the electrochemical incineration of bromophenol blue on boron-doped diamond anode, Diamond Relat. Mater. 50 (2014) 1–8.
[23] S. Veloutsou, E. Bizani, K. Fytianos, Photo-Fenton decomposition of β-blockers atenolol and metoprolol; study and optimization of system parameters and identification of intermediates, Chemosphere 107 (2014) 180–186.

[24] E.L. Foletto, S. Battiston, J.M. Simões, M.M. Bassaco, L.S.F. Pereira, É.M. de Moraes Flores, E.I. Müller, Synthesis of $ZnAl_2O_4$ nanoparticles by different routes and the effect of its pore size on the photocatalytic process, Microporous Mesoporous Mater. 163 (2012) 29–33.
[25] E.L. Foletto, J.M. Simões, M.A. Mazutti, S.L. Jahn, E.I. Muller, L.S.F. Pereira, E.M.M. Flores, Application of Zn_2SnO_4 photocatalyst prepared by microwave-assisted hydrothermal route in the degradation of organic pollutant under sunlight, Ceram. Int. 39 (2013) 4569–4574.
[26] C.G. Anchieta, E.C. Severo, C. Rigo, M.A. Mazutti, R.C. Kuhn, E.I. Muller, E.M.M. Flores, R.F.P.M. Moreira, E.L. Foletto, Rapid and facile preparation of zinc ferrite ($ZnFe_2O_4$) oxide by microwave-solvothermal technique and its catalytic activity in heterogeneous photo-Fenton reaction, Mat. Chem. Phys. 160 (2015) 141–147.
[27] B.D. Cullity, S.R. Stock, Elements of X-ray Diffraction, third ed., Prentice-Hall Inc, New Jersey, 2001.
[28] R.M. Silverstein, F.X. Webster, D.J. Kiemle, Spectrometric Identification of Organic Compounds, seventh ed., J. Wiley & Sons, New York, NY, 2005.
[29] S. Brunauer, P.H. Emmett, E. Teller, Adsorption of gases in multimolecular layers, J. Am. Chem. Soc. 60 (1938) 3091–3318.
[30] L. Lu, Y. Ma, M. Kumar, J.G. Lin, Photo-Fenton pretreatment of carbofuran—Analyses via experimental design, detoxification and biodegradability enhancement, Sep. Purif. Technol. 81 (2011) 325–331.
[31] A.D. Bokare, W. Choi, Review of iron-free Fenton-like systems for activating H_2O_2 in advanced oxidation processes, J. Hazard. Mater. 275 (2014) 121–135.
[32] C. Orbeci, I. Untea, G. Nechifor, A.E. Segneanu, M.E. Craciun, Effect of a modified photo-Fenton procedure on the oxidative degradation of antibiotics in aqueous solutions, Sep. Purif. Technol. 122 (2014) 290–296.
[33] G.L. Dotto, L.A.A. Pinto, Adsorption of food dyes onto chitosan: Optimization process and kinetic, Carbohydr. Polym. 84 (2011) 231–238.
[34] T.V. Rêgo, T.R.S. Cadaval Jr, G.L. Dotto, L.A.A. Pinto, Statistical optimization, interaction analysis and desorption studies for the azo dyes adsorption onto chitosan films, J. Colloid Interface Sci. 411 (2013) 27–33.
[35] N.M. Mahmoodi, Zinc ferrite nanoparticle as a magnetic catalyst: Synthesis and dye degradation, Mater. Res. Bull. 48 (2013) 4255–4260.
[36] C.G. Anchieta, D. Sallet, E.L. Foletto, S.S. da Silva, O. Chiavone-Filho, C.A.O. do Nascimento, Synthesis of ternary zinc spinel oxides and their application in the photodegradation of organic pollutant, Ceram. Int. 40 (2014) 4173–4178.
[37] K.S.W. Sing, D.H. Everet, R.A.W. Haul, L. Moscou, R.A. Pieroti, J. Rouquerol, T. Siemieniewska, Reporting physisorption data for gas/solid systems with special reference to the determination of surface area and porosity, Pure Appl. Chem. 57 (1985) 603–619.
[38] R. Andreozzi, V. Caprio, A. Insola, R. Marotta, Advanced oxidation processes (AOP) for water purification and recovery, Catal. Today 53 (1999) 51–59.
[39] Y. Gao, H. Gan, G. Zhang, Y. Guo, Visible light assisted Fenton-like degradation of rhodamine B and 4-nitrophenol solutions with a stable poly-hydroxyl-iron/sepiolite catalyst, Chem. Eng. J. 217 (2013) 221–230.
[40] A.N. Soon, B.H. Hameed, Degradation of Acid Blue 29 in visible light radiation using iron modified mesoporous silica as heterogeneous Photo-Fenton catalyst, Appl. Catal., A: Gen. 450 (2013) 96–105.
[41] C. Yaman, G. Gündüz, A parametric study on the decolorization and mineralization of C.I. Reactive Red 141 in water by heterogeneous Fenton-like oxidation over FeZSM-5 zeolite, J. Environ. Health Sci. Eng. 13 (2015) 7.